A MEDIAL MAP CAPTURING THE ESSENTIAL GEOMETRY OF ORGANS

Sergio Vera[⋆†] *Miguel A. González*[⋆] *Debora Gil*[†]

[⋆] Alma IT Systems
[†] Computer Vision Center, Comp. Science Dep., Universitat Autònoma de Barcelona

ABSTRACT

Medial representations are powerful tools for describing and parameterizing the volumetric shape of anatomical structures. Accurate computation of one pixel wide medial surfaces is mandatory. Those surfaces must represent faithfully the geometry of the volume. Although morphological methods produce excellent results in 2D, their complexity and quality drops across dimensions, due to a more complex description of pixel neighborhoods.

This paper introduces a continuous operator for accurate and efficient computation of medial structures of arbitrary dimension. Our experiments show its higher performance for medical imaging applications in terms of simplicity of medial structures and capability for reconstructing the anatomical volume.

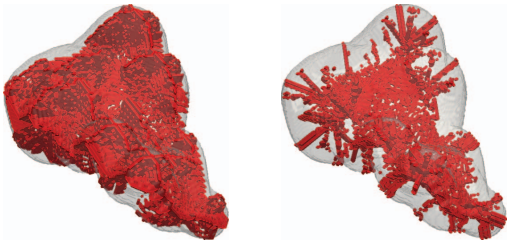
Index Terms— Medial Surface Representation, Volume Reconstruction

1. INTRODUCTION

Medial representations have gained increasing popularity for describing and segmenting anatomical structures. Techniques such as M-Reps [1] and CM-Reps [2] have shown the potential to describe complex shapes in a versatile manner. Deformable medial modelling has been used in a variety of medical imaging analysis applications, including computational neuroanatomy [3], 3D cardiac modelling [4, 5], and cancer treatment planning [6].

Medial representations model anatomical volumes by explicitly defining a medial manifold and its radial perpendicular coordinate [7]. Any medial manifold used to (re)generate anatomical volume must be simple enough to allow an easy generation of the radial axis, but complete enough to allow a satisfactory reconstruction of the volume.

Most methods for medial surface computation are based on morphological (ordered) thinning operations on either the original volume or the distance map to its boundary. In any case, they require the definition of a neighborhood set and surface conditions for the removal of simple voxels (those that do not alter the topology if removed) that do not lie on a surface. The complexity of neighborhood definition and surface tests increases exponentially with the dimension of the embedding space [8]. Additionally, small changes in those tests or in the order in which voxels are traversed, generates completely different surfaces (as illustrated in Fig. 1).



(a) (b)

Fig. 1: Medial surfaces obtained using a 6-connected neighborhood, (a), and a 26 connected neighborhood, (b).

A completely different approach is the two-fold method introduced in [9]. In this work, medial structures are computed applying Non Maxima Suppression (NMS) to a medial map based on a normalized ridge detector. Although NMS binarization proved to surpass standard thinning methods, a main concern is the introduction of internal holes in medial surfaces and a significant drop of the response at self-intersections.

The present work focuses on the definition of a medial map capable of producing complete medial surfaces reaching a good compromise between simplicity of the medial geometry and its ability to reconstruct the whole anatomical volume. After thorough analysis of the main properties and shortcomings of existing ridge operators, we introduce a medial map based on ridge detectors that combines the advantages of steerable filters and level sets geometry. We call this medial map Geometric Steerable Medial Map, GSM2. A database of 3D liver segmentations [10] is used as a benchmark to evaluate the degree of similarity between volumes obtained from medial surfaces. Our experiments show the higher performance of our approach compared to morphological methods.

This research has been funded by the Spanish projects TIN2009-13618, CSD2007-00018 and 2009-TEM-00007. The last author has been supported by the Ramon y Cajal Program

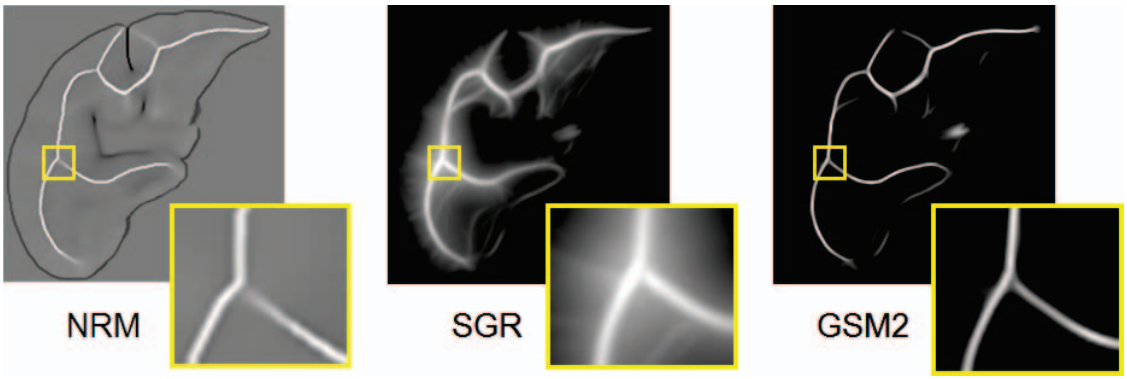


Fig. 2: Performance of different ridge operators. Normalized Ridge Map (left), Steerable Gaussian Ridge (center) and Geometric Steerable Medial Map (right).

2. A GEOMETRIC STEERABLE MEDIAL MAP

Distance maps are a key element for obtaining medial maps, since, by definition, their maximum values are located at central voxels corresponding to the medial structure. Distance maps can be used directly to generate skeletons ([11]) but the ridges of the distance map have show superior power to identify medial voxels [9]. In image processing, ridge detectors are based either on level sets geometry or image intensity profiles.

The map described in [12], defines ridges as lines joining points of maximum curvature of the distance map level sets. It is computed using the maximum eigenvector of the structure tensor of the distance map as follows.

Let $\vec{V}$ be the eigenvector of principal eigenvalue of the structure tensor and consider its reorientation along the distance gradient, $\vec{V} = (P, Q, R)$, given as:

$$\vec{V} = \text{sign}(< \vec{V} \cdot \nabla D >) \cdot \vec{V}$$

for $< \cdot >$ the scalar product. The ridgeness measure [12] is given by the divergence:

$$NRM := \text{div}(\vec{V}) = \partial_x P + \partial_y Q + \partial_z R \qquad (1)$$

The above operator assigns positive values to ridge pixels and negative values to valley ones.

A main advantage is that NRM $\in [-N, N]$ for N the dimension of the volume. In this way, it is possible to set a threshold common to any volume for detecting significant ridges and, thus, points highly likely to belong to the medial surface. However, by its geometric nature, NRM has two main limitations. In order to be properly defined, NRM requires that the vector $\vec{V}$ uniquely defines the tangent space to image level sets. Therefore, the operator achieves strong responses in the case of one-fold medial manifolds, but significantly drops anywhere two or more medial surfaces intersect each other. Additionally, NRM responses are not continuous maps but step-wise almost binary images (see Fig.2 left). Such discrete nature of the map hinders the performance of the NMS binarization step that removes some internal voxels of the medial structure and, thus, introduces holes in the final medial surface.

On the other side, ridge maps based on image intensity are computed by convolution with a bank of steerable filters. Each filter is defined by 2nd derivatives of (oriented) anisotropic 3D Gaussian kernels:

$$g_\sigma^\Theta = g_{(\sigma_x,\sigma_y,\sigma_z)}^{(\theta,\phi)} = \frac{1}{(2\pi)^{3/2}\sigma_x\sigma_y\sigma_z} e^{-\left(\frac{\tilde{x}^2}{2\sigma_x^2}+\frac{\tilde{y}^2}{2\sigma_y^2}+\frac{\tilde{z}^2}{2\sigma_z^2}\right)}$$

for $(\tilde{x}, \tilde{y}, \tilde{z})$ the coordinates given by a rotations of angles θ and ϕ that transform the z-axis into the unitary vector $(cos(\phi)cos(\theta), cos(\phi)sin(\theta), sin(\phi))$. In order to detect sheet-like ridges, the scales are set to $\sigma_z < \sigma_x = \sigma_y$.

The second partial derivative along the z axis constitutes the principal kernel for computing ridges:

$$\partial_z^2 g_\sigma^\Theta = (\tilde{z}^2/\sigma_z^4 - 1/\sigma_z^2) g_\sigma^\Theta$$

The response of the operator Steerable Gaussian Ridge (SGR) is calculated as the maximum response for a discrete sampling of the angulation:

$$SGR := \max_{i,j} \left(D * \partial_z^2 g_\sigma^{\Theta_{i,j}} \right) \qquad (2)$$

for $\Theta_{i,j}$ given by $\theta_i = \{\frac{i\pi}{N}, i = 1..N\}$ and $\phi_j = \{\frac{j\pi}{M}, j = 1..M\}$.

A main advantage of using steerable filters is that their response provides continuous maps which ensure completeness of the surfaces obtained by NMS binarization. Besides, since they decouple the space of possible orientations for medial surfaces, their response does not decrease at self-intersections (see Fig.2 left and center). Their main counterpart is that their response is not normalized, so setting the threshold for NMS binarization becomes a delicate issue.

The analysis above shows that geometric and intensity methods have complementary advantages and shortcomings.

Therefore we propose combining them into the following Geometric Steerable Medial Map (GSM2):

$$GSM2 := SGR(NMR) = \max_{i,j} \left(NRM * \partial_z^2 g_\sigma^{\Theta_{i,j}} \right) \quad (3)$$

The advantages of GSM2 are two-fold. On one hand, steerable filters provide a continuous approximation to NMR semi-discrete maps with a more uniform response at self-intersecting points. On the other hand, because NMR maps have a sharp response at central voxels, GSM2 still provides a highly selective response at ridges. In this manner GSM2 generates medial maps with good combination of specificity in detecting medial voxels while having good characteristics for NMS binarization, which does not introduce internal holes (Fig. 2 right).

3. VALIDATION EXPERIMENTS

In order to provide a real scenario for the reconstruction tests we use 14 livers from the SLIVER07 challenge [10] as a source of anatomical volumes. We have applied GSM2 using $\sigma = 0.5$, $\rho = 1$ for computing structure tensors in NMR and $N = M = 8$ orientations for SGR. In order to compare to morphological methods, we also applied an ordered thinning using a 6-connected neighborhood (labeled Th_6) described in [13], a 26-connected neighborhood (labeled Th_{26}) described in [11] and a pruning of the 26-connected neighborhood (labeled Th_{26P}).

As some of the medial surface techniques include some sort of pruning, our experiments will focus on evaluating how the pruning affects the generation of reconstructed volumes. Volumes are reconstructed from the computed medial surfaces by applying the inverse medial transform. Comparisons with the original shape are based on volumetric measures (Volume Overlap Error (VOE), Relative Volume Difference (RVD) and Dice coefficient) and symmetric surface distances(Average (AvSD), and Maximum (MxSD)) [10]. Aside from dice coefficient, lower metric values indicate better reconstruction capability.

Table 1 reports statistical ranges for all methods and measures computed for the 14 livers. Although, there are not significant differences among methods, our approach and the pruned thinning have better reconstruction power. Additionally in the case of thinning based methods, medial manifolds have a more complex geometry than GSM2 and might include extra structures and self intersections (Fig. 3). In medical applications such extra structures might hinder the identification of abnormal or pathological structures. This is not the case for GSM2 surfaces as exemplified in Fig. 4. The oversized superior lobe on the right liver is captured by the presence of an unusual medial manifold configuration.

4. CONCLUSIONS

In order to provide more intuitive and easily interpretable representations of complex organs, medial manifolds should reach a compromise between simplicity in geometry and capability for restoring the anatomy of the organ. The method presented in this paper allows the computation of medial manifolds without relying in morphological methods nor neighbourhood or surface tests. Additionally, it can be seamless implemented regardless of the dimension of the embedding space. The resulting medial surfaces are of greater simplicity than the generated by thinning methods. Although having this minimalistic property, the resulting manifolds can be used to recalculate the original volume with slightly better reconstructions than existing methods.

5. REFERENCES

[1] S.M. Pizer and P.T. Fletcher et al., "Deformable M-Reps for 3D medical image segmentation," *Int. J. Comp. Vis.*, vol. 55, no. 2, pp. 85–106, 2003.

[2] P.A. Yushkevich, "Continuous medial representation of brain structures using the biharmonic PDE," *NeuroImage*, vol. 45, no. 1, pp. 99–110, 2009.

[3] Martin Styner, Jeffrey A. Lieberman, Dimitrios Pantazis, and Guido Gerig, "Boundary and medial shape analysis of the hippocampus in schizophrenia," *Medical Image Analysis*, vol. 8, no. 3, pp. 197–203, 2004.

[4] H. Sun, B.B. Avants, A.F. Frangi, F. Sukno, J.C. Gee, and P.A. Yushkevich, "Cardiac medial modeling and time-course heart wall thickness analysis," in *MICCAI*, 2008, vol. 5242, pp. 766–773.

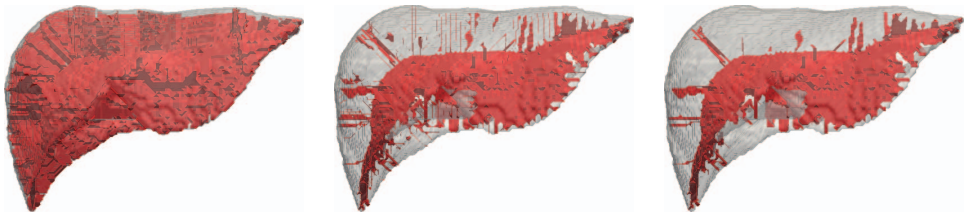
[5] H. Sun, A. F. Frangi, H. Wang, and et al, "Automatic cardiac mri segmentation using a biventricular deformable medial model," in *MICCAI*. 2010, vol. 6361, pp. 468–475, Springer.

[6] Joshua Stough, Robert Broadhurst, Stephen Pizer, and Edward Chaney, "Regional appearance in deformable model segmentation," vol. 4584, pp. 532–543, 2007.

[7] H. Blum, *A transformation for extracting descriptors of shape*, MIT Press, 1967.

[8] T. C. Lee, R. L. Kashyap, and C. N. Chu, "Building skeleton models via 3-D medial surface axis thinning algorithms," *Grap. Mod. Imag. Process.*, vol. 56, no. 6, pp. 462–478, 1994.

[9] S. Vera, D. Gil, A. Borràs, X. Sánchez, F. Pérez, M. G. Linguraru, and M. A. González Ballester, "Computation and evaluation of medial surfaces for shape representation of abdominal organs," in *MICCAI Abdominal Imaging*. 2011, vol. 7029 of *LNCS*, pp. 223–230, Springer.



(a) (b) (c)

Fig. 3: Medial Manifolds of a healthy liver generated with morphological methods. Th_6 (left), Th_{26} (center), Th_{26P} (right).

	$GSM2$	Th_6	Th_{26}	Th_{26P}
Volume Error				
VOE	7.9641 ± 1.6973	8.8396 ± 1.7287	8.2471 ± 1.7235	7.8378 ± 1.6778
RVD	8.4925 ± 2.0314	9.1014 ± 2.1014	8.9602 ± 2.0857	7.8618 ± 2.2303
Dice	0.9585 ± 0.0092	0.9535 ± 0.0095	0.9569 ± 0.0094	0.9591 ± 0.0091
Surface Dist.				
AvSD	0.7969 ± 0.0581	0.8876 ± 0.0624	0.8278 ± 0.0546	0.7831 ± 0.0504
MxSD	5.6100 ± 2.6783	6.0037 ± 2.5859	5.5222 ± 2.5562	5.5748 ± 2.4864

Table 1: Errors in reconstruction.

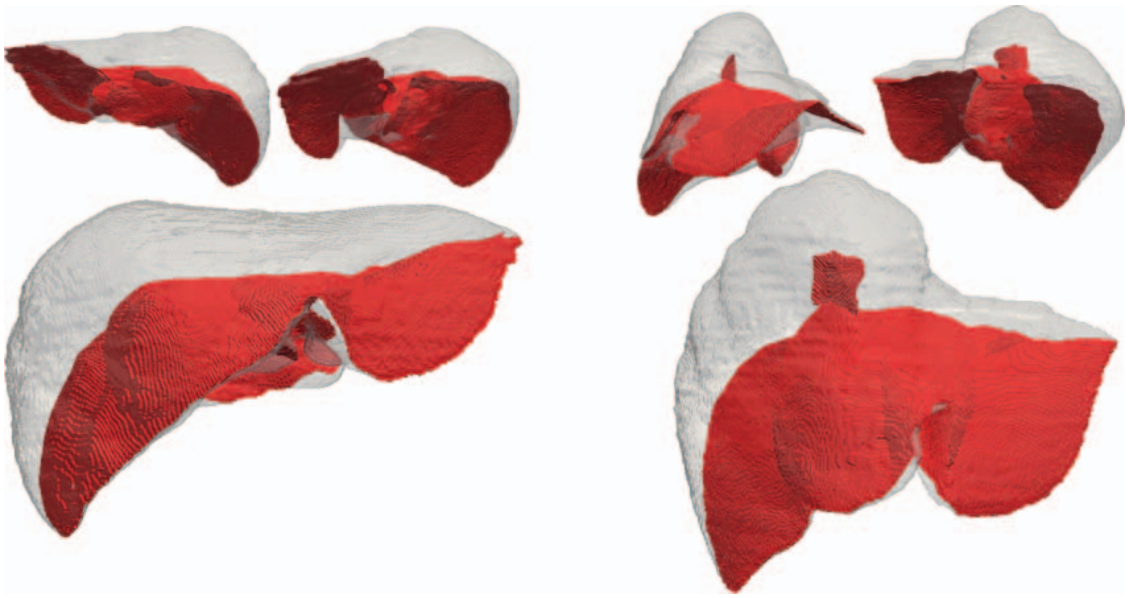


Fig. 4: Medial Manifolds of a healthy liver (left) and a liver with an unusual lobe (right).

[10] T. Heimann, B. van Ginneken, M. A. Styner, Y. Arzhaeva, and V. Aurich, "Comparison and evaluation of methods for liver segmentation from CT datasets," *IEEE Trans. Med. Imag.*, vol. 28(8), pp. 1251–1265, 2009.

[11] C. Pudney, "Distance-ordered homotopic thinning: A skeletonization algorithm for 3D digital images," *Comp. Vis. Imag. Underst.*, vol. 72(2), pp. 404–13, 1998.

[12] A.M. Lopez, F. Lumbreras, J. Serrat, and J.J. Villanueva, "Evaluation of methods for ridge and valley detection," *IEEE Trans. Pat. Ana. Mach. Intel.*, vol. 21, no. 4, pp. 327–335, 1999.

[13] Sylvain Bouix and Kaleem Siddiqi, "Divergence-based medial surfaces," in *ECCV*, 2000, pp. 603–618.